Towards a mechanistic understanding of nanoparticle behavior using zebrafish

Arias Alpizar, G.

Chapter 3

Stabilin-1 is required for the endothelial clearance of small anionic nanoparticles

Published:

Arias-Alpizar, G.; Koch, B.; Hamelmann, N. M.; Neustrup, M. A.; Paulusse, J. M. J.; Jiskoot, W.; Kros, A.; Bussmann, J., Stabilin-1 is required for the endothelial clearance of small anionic nanoparticles. Nanomedicine 2021, 34, 102395.

Image: A new Stabilin ligand, lipopolysaccharide (in green) removed from circulation by scavenging endothelial cells, macrophages in magenta

3.1 Abstract

Clearance of nanoparticles (NPs) after intravenous injection -mainly by the liver- is a critical barrier for the clinical translation of nanomaterials. Physicochemical properties of NPs are known to influence their distribution through cell-specific interactions; however, the molecular mechanisms responsible for liver cellular NP uptake are poorly understood. Liver sinusoidal endothelial cells and Kupffer cells are critical participants in this clearance process. Here we use a zebrafish model for liver-NP interaction to identify the endothelial scavenger receptor Stabilin-1 as a non-redundant receptor for the clearance of small anionic NPs. Furthermore, we show that physiologically, Stabilin-1 is required for the removal of bacterial lipopolysaccharide (LPS/endotoxin) from circulation and that Stabilin-1 cooperates with its homolog Stabilin-2 in the clearance of larger (~100 nm) anionic NPs. Our findings allow optimization of anionic nanomedicine biodistribution and targeting therapies that use Stabilin-1 and -2 for liver endothelium-specific delivery.

3.2 Introduction

Clinical application of nanoparticles (NPs) after intravenous (*i.v.*) administration and delivery of their cargo (*i.e.* drugs, DNA, RNA) are hampered by the rapid sequestration of NPs, mainly by cells in the liver.[1, 2] Consequently, removal of NPs with sizes above the renal filtration limit (~5.5 nm) from blood plasma,[3] leads to the accumulation of most NPs in the liver. Kupffer cells (KCs), the tissue-specific macrophages that are located on the luminal side of the liver capillary vasculature (*i.e.* sinusoids), recognize and internalize NPs and were long thought to be the only liver cell type responsible for NP clearance *in vivo*. However, recent studies on the cellular distribution of NPs within the liver have revealed important contributions of B-lymphocytes, hepatocytes, hepatic stellate cells and especially liver sinusoidal endothelial cells (LSECs).[4]

The relative contribution of KCs and LSECs to the clearance of circulating NPs depends mainly on size. Phagocytosis by KCs is responsible for clearance of particles with a size >500 nm.[5, 6] These NPs are captured by KCs either directly through endocytic receptors on their surface (such as scavenger and mannose receptors), or indirectly, after binding of serum proteins to the NP surface (*i.e.* opsonization) and subsequent recognition of the bound proteins by Fc- and complement receptors.[7] Compared to KCs, clearance by the more numerous LSECs (present in an approximately 1:2 ratio)[4] is largely dependent on clathrin-mediated endocytosis and is limited to particles with a size <500 nm.[8] Although for LSECs the molecular mechanisms leading to cellular NP uptake are less well understood, it is known that LSECs internalize biological colloids – such as viral particles,[9] bacterial lipopolysaccharide (LPS),[10, 11] oxidized lipoprotein particles[11, 12] and immune complexes[13] – at a similar rate to, or exceeding uptake by KCs.

Analysis and identification of the molecular mechanisms that mediate NP clearance will help in the challenging task of translation of nanomedicines. The analysis of LSEC function is complicated due to the rapid dedifferentiation of LSECs *in vitro*[14] and relies, consequently, on *in vivo* animal models. Recently, we have established an *in vivo* zebrafish model for NP clearance and have identified a cell type homologous to LSECs in the early zebrafish embryo.[15] These cells, which we named scavenging endothelial cells (SECs), in analogy with previously identified non-mammalian LSEC homologs[16] – are not located in the liver (as in mammals). Instead, they line the first embryonic veins and provide blood clearance before the liver vasculature becomes functional. Zebrafish is a

convenient model owing to their ease of genetic manipulation and optical transparency in embryonic stages that provides the opportunity to combine genome-editing techniques and non-invasive microscopy imaging in real-time. Furthermore, zebrafish embryos are used to screen and optimize formulations prior to clinical studies. Remarkably, the clearance function of SECs and their gene expression signature in the zebrafish are comparable to those of the mammalian LSECs, as demonstrated by the presence of several endocytic receptors including several scavenger receptors.[17]

LSEC-specific scavenger receptors are prominent candidates for mediating NP clearance in this cell type, since they have been reported to interact and endocytose a wide range of ligands including modified lipoprotein particles,[12] bacterial and viral pathogens,[18] and exosomes.[19] One of the LSEC-specific scavenger receptors – Stabilin-2 – has been found to bind and internalize apoptotic bodies[20] as well as exogenous ligands, such as antisense oligonucleotides[21] and NPs.[22] Indeed, by generating a zebrafish *stab2* knockout line, we showed that Stabilin-2 is an important receptor for SEC-mediated clearance of anionic NPs.[15] However, we also observed that some negatively charged NPs were not only dependent on this receptor for clearance, demonstrated by the uptake of NPs in the SECs even in the absence of a functional Stabilin-2.

In this study, we identify a requirement for the *stab2* homolog, Stabilin-1 (encoded by *stab1* gene), in the removal of small (~6-30 nm) NPs from circulation. These two scavenger receptors have highly similar domain structure, consistent with the binding of Stabilin-1 to most (but not all) Stabilin-2 ligands *in vitro*,[23] suggestive of functional redundancy.[24] In addition, we generated *stab1/stab2* double knockout zebrafish embryos to provide evidence that Stabilin receptors complement each other in NP clearance of larger NPs (~100 nm size), as well as in the removal of bacterial LPS from the circulation. Differential scavenging function between Stabilin-1 and Stabilin-2 suggests size as a determinant for receptor specificity.

3.3 Results

Generation and characterization of *stab1* and *stab2* double knockout zebrafish

Liver endothelium is characterized by the presence of scavenger receptors strongly expressed on the membrane cell surface. Given that the clearance of some anionic NPs are not exclusively dependent on the scavenging function of Stabilin-2,[15] we hypothesized that one or more other scavenger receptor(s) expressed in LSECs might be involved in the removal of NPs. To identify additional clearance receptors, we first analyzed the RNA expression of all scavenger receptors in LSECs from mice liver, based on published single-cell RNA sequencing datasets,[25-27] (**Supplementary Table 1**). Although this analysis revealed that *Stab2* is the most abundant scavenger receptor expressed in LSECs, the expression of seven other scavenger receptors (*Msr1, Scarb1, CD36, Scarf1, Mrc1, CXCl16* and *Stab1*) was consistently observed. Of these, the mannose receptor (*Mrc1*) and *Stab1* are the most abundant scavenger receptors expressed by LSECs besides *Stab2*. We previously reported that the zebrafish orthologues of these genes (*mrc1a* and *stab1*) are also highly expressed on SECs.[15] Since Stabilin-1 binds similar ligands as Stabilin-2,[23] we further analyzed the role of this receptor in NP clearance.

To this end, we generated a zebrafish *stab1* mutant line through CRISPR/Cas mutagenesis (guide RNA sequence in **Supplementary Table 2**). In this strain (*stab1*^{ibl3}), a deletion of one nucleotide causes a frame-shift, leading to a premature stop codon after amino acid number eighty-five. The predicted gene product is a truncated protein lacking most conserved domains, including the fasciclin, EGF-like and LINK domains (**Figure 1a**). This gene knockout approach allow us to study the biodistribution of NPs in zebrafish embryo and to compare the clearance by SECs in the presence and/or absence of functional Stabilin receptor(s). To study the combined contributions of Stabilin-1 and Stabilin-2, embryos with mutations in both *stab1* and *stab2 (stab*^{DKO}*)* were also generated intercrossing *stab1*^{ibl3} and *stab2*^{ibl2} carriers. Characterization of the generated mutants was performed by whole-mount *in situ* hybridization (ISH). Using antisense RNA probes we found a strong reduction of *stab1* expression in *stab1*^{ibl3} homozygous mutant embryos, consistent with nonsense-mediated decay (NMD) of the mutant RNA, whereas *stab2* and *mrc1a* expression were unaffected, indicating normal SEC differentiation (**Figure 1b**).

In *stab*^{DKO} embryos, expression of both *stab1* and *stab2* was also reduced through NMD. Of note, *stab2* expression was found to be slightly increased in *stab*^{DKO} compared to the signal in *stab2* mutant embryos. Importantly, *mrc1a* expression in *stab*^{DKO} embryos was maintained, indicating that SEC differentiation occurred even after the combined loss of *stab1* and *stab2.* Homozygous *stab1* zebrafish mutants develop a normal blood and lymphatic vascular system and we did not observe the previously described defects in lymphatic development induced by morpholino oligonucleotide-mediated after *stab1* knockdown[28] (**Figure 1c**). *Stab1* mutant embryos develop without obvious morphological defects into viable and fertile adults (**Figure 1d**) similar to *stab2* mutant zebrafish, as well as adult Stab1 knockout mice. Strikingly, although Stab1/2 double knockout mice display reduced viability due to kidney failure, adult *stab*^{DKO} zebrafish did not show increased mortality or pathology.

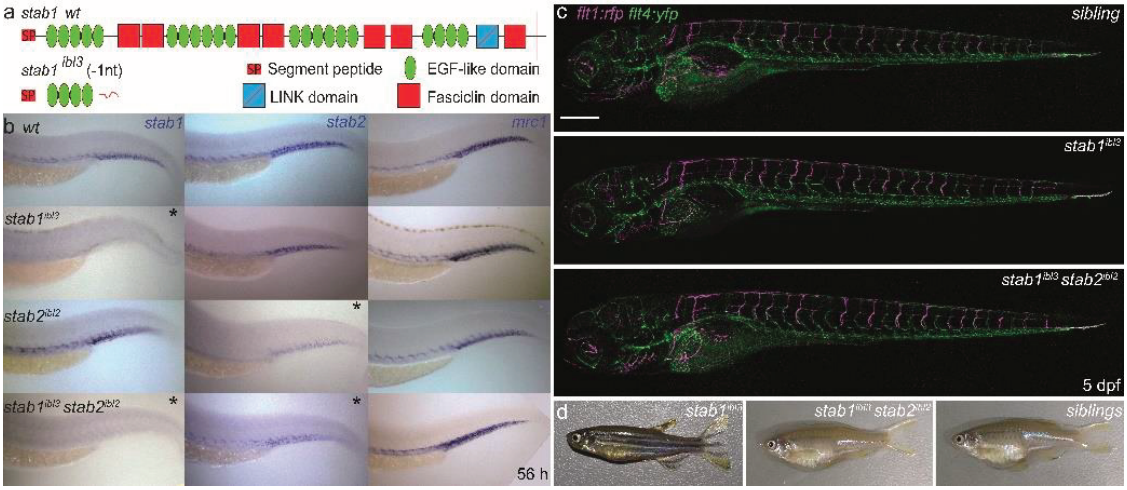

Figure 1. Generation and characterization of *stab1* and *stab1/stab2* mutants. (a) Schematic representation of a *stab1* domain structure predicted to be expressed from the wt Stabilin-1 and the *stab1*^{ibl3} allele. **(b)** *In situ* hybridization (ISH), mRNA expression of *stab1, stab2,* and *mrc1* in wt, *stab1*^{ibl3}, *stab2*^{ibl2} single mutants and s*tab1*^{ibl3}*stab2*^{ibl2} double mutant. *Reduced expression. **(c)** Tg(*fli1:*RFP *fli4:*YFP) *stab1*^{ibl3} mutant, s*tab1*^{ibl3}*stab2*^{ibl2} double mutant, and sibling at 5 dpf. Scale bar: 250 µm. **(d)** Representative fertile adult female *stab1*^{ibl3} single mutant, *stab1*^{ibl3}*stab2*^{ibl2} double mutant and sibling zebrafish.

Identification of Stabilin-1 function in the clearance of anionic NPs

Previously we found that two types of NPs were efficiently cleared by SECs even in the absence of *stab2* expression.[15] Specifically, these were quantum dots (Qdots) with a negatively charged surface coating and Cowpea Chlorotic Mottle

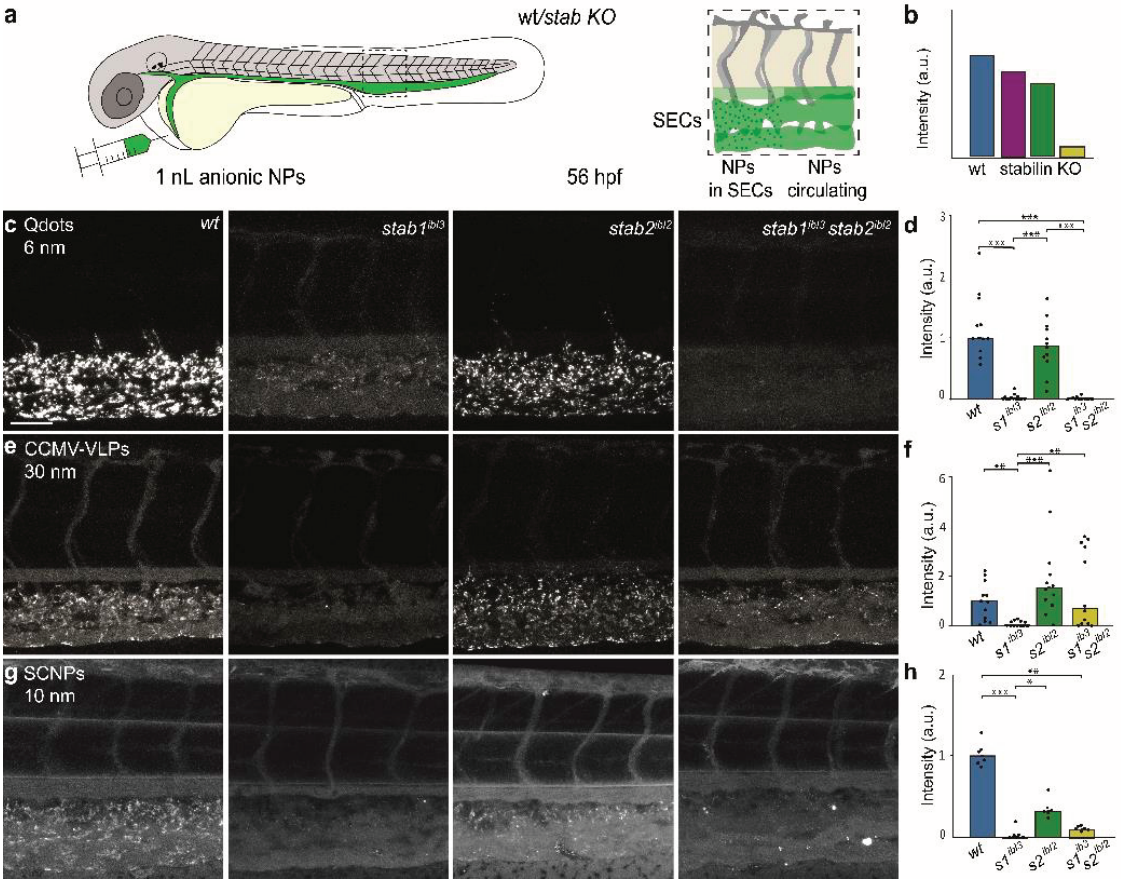

Figure 2. Clearance of small anionic NPs occurs mainly through Stabilin-1. (a) Schematics showing the site of injection within a 56 hours post fertilization (hpf) wt or *stab* knockout zebrafish. In a box, the caudal vein region, where SECs expressing Stabilins are located, a representation of NP circulating or cleared by SECs. **(b)** Representative graph comparing intensity of fluorescent NPs in wt and *stab* mutants. **(c-d)** Tissue level view and quantification of fluorescently labeled Qdots. **(e-f)** CCMV-VLP **(g-h)** SCNPs. After *i.v.* injection (1 nL) in wt *(AB/TL), stab1*^{ibl3}*, stab2*^{ibl2} single mutants and *stab1*^{ibl3}*stab2*^{ibl2} double mutants at 1-1.5 hpi. Scale bar: 50 µm. Bar height represents median values, dots represent individual data points, and brackets indicate significant values (*P< 0.05, **P<0.01, ***P<0,001) based on Kruskal-Wallis tests followed by two-tailed Dunn's tests with Bonferroni correction.

Virus derived virus-like particles (CCMV-VLPs), which are non-enveloped protein capsids with a hexagonal closed packed structure.[29] As most viruses, these VLPs have a negative surface charge. Biodistribution of the Qdots was unchanged in *stab2* mutants, while only a small reduction in the clearance of CCMV-VLPs was observed. The clearance of these two particle types, however, is apparently mediated through scavenger receptors, since it was completely inhibited by pre-injection with the general scavenger receptor inhibitor, dextran sulfate. Therefore, we injected fluorescently labeled Qdots and CCMV-VLP *i.v.*

into the duct of Cuvier of wildtype (wt), *stab1*^{ibl3}, *stab2*^{ibl2} and *stab*^{DKO} zebrafish embryos at 56 hours post fertilization (hpf) and subsequently imaged their biodistribution with confocal microscopy. The resulting accumulation of NP fluorescence representing SEC-mediated clearance was quantified (see **Methods** for details) on a cellular level in the caudal region of the zebrafish tail (**Figure 2a-b**). Importantly, this region also contains plasma-exposed macrophages, commonly known to remove NPs from circulation and analogous to the mammalian Kupffer cells (exemplified in **Supplementary Figure 1**). Strikingly, for both Qdots and CCMV-VLPs, we observed a strong reduction in NP clearance in both *stab1* ^{ibl3} mutants and *stab*^{DKO} embryos indicating a dominant role for Stabilin-1 in the clearance of these NP types (**Figure 2c-f** and **Supplementary Figure 2a-b**). NPs that were cleared mainly through Stabilin-1 differ in their composition (inorganic *vs.* viral capsids) and surface chemistry, and were also chemically distinct from the NPs cleared mainly through Stabilin-2 (which included lipid and polymeric particles).

The difference in surface chemistry of all NPs studied suggests a more general mechanism where particle size might be an important factor for receptor specificity. To further strengthen this hypothesis, we next injected chemically distinct (polymeric) small NPs. To this end, fluorescently labeled anionic single-chain polymeric NPs (SCNPs) were used. SCNPs are a polymeric NP type which consist of biodegradable polymer chains that are covalently cross-linked and folded to form a small particle.[30] The resulting NP size is defined by the length of the polymer chain and can be used to obtain small, uniform polymer NPs of 10-20 nm. Injection of ~10 nm SCNPs in the zebrafish embryo revealed that clearance of these particles occurred through SECs as expected. Importantly, SCNP clearance was strongly affected in *stab1* mutants, similar to Qdots and CCMV-VLPs (**Figure 2g-h** and **Supplementary Figure 2c**). This results indicates that - for negatively charged NPs – size, rather than chemical composition, is a predominant factor for receptor specificity.

Stabilin-1 and Stabilin-2 are complementary receptors in the clearance of anionic NPs by SECs

Previous studies on the biodistribution of polymer- and lipid-based NPs including polymersomes,[15, 31] fibrillar supramolecular polymers,[32] solid polystyrene (PS) NPs and liposomes[15] in zebrafish *stab2* mutants revealed a residual uptake of NPs in SECs in the absence of *stab2* expression. Common characteristics of these NPs were a negative surface, but these NPs differed in size, shape, composition and rigidity. To investigate a complementary role of

Stabilin-1 to Stabilin-2 in the clearance of NPs ~100 nm, we injected negatively charged DOPG-liposomes and polymersomes in *stab*^{DKO} embryos. Interestingly, the clearance of both NPs in *stab*^{DKO} embryos was strongly affected, more than that observed in *stab2* single mutants. The loss of a functional Stabilin-1 did not affect the biodistribution of these particles compared to wt embryos (**Figure 3a-d** and **Supplementary Figure 3a-b**), in striking contrast to the biodistribution of the smaller NPs. This indicates a cooperative role of Stabilin-1 and Stabilin-2 in NP clearance, consistent with their highly similar ligand profile.[23]

We next analyze the behavior of more rigid solid NPs. Therefore, we used anionic poly(D,L-lactide-co-glycolide) (PLGA) NPs and spherical silica NPs (siNPs) due to their relevant importance in drug delivery or biomedical imaging agents applications.[33, 34] Similar to polymersomes and DOPG-liposomes, anionic PLGA NPs and siNPs are cleared through SECs in wt zebrafish. Their biodistribution remained unchanged in *stab1* mutants, but clearance was strongly affected in *stab2* mutants, and even more in *stab*^{DKO} mutants (**Figure 3e-h** and **Supplementary Figure 3c-d**). Interestingly, for the PLGA NPs, the absence of SEC clearance resulted in increased macrophage uptake (indicated by white arrows in **Figure 3e,g** and **Supplementary Figure 1**). The absence of molecular interactions between NPs for most of the ~100 nm NPs and SECs in the *stab*^{DKO} embryos is evidence of a combined contribution of Stabilin-1 and Stabilin-2, where Stabilin-2 is the predominant receptor involved in the clearance in this size range. However, this contribution seems to be a more complex process that depends not only on size but also on the particle composition. We observed this behavior for anionic NP type (polystyrene NPs) of different sizes (**Supplementary Figure 4a**). In this case, we first qualitatively confirmed SEC-uptake of these particles through co-injection with fluorescently labeled hyaluronic acid (fluoHA), a Stabilin-2 ligand and a marker for SEC endocytosis (**Supplementary Figure 4b-c**). SEC clearance is only partly affected in *stab*^{DKO} mutants, indicating the presence of at least one additional clearance receptor besides Stabilin-1 and Stabilin-2 (**Supplementary Figure 4d-g**).

Identification of an endogenous Stabilin ligand: bacterial LPS

Clearance of synthetic nanoparticles can only be reflective of physiological mechanisms that are required for the removal of naturally occurring particles in the 10 nm to 200 nm size range. We therefore sought to identify naturally occurring circulating particles of this dimension as a probable physiologic Stabilin ligands. One such ligand is LPS, which is the main component of the outer membrane of Gram-negative bacteria with the lipid A portion, an anchor in the

bacterial cell wall, that provides toxicity and activates immune responses in mammals.[35] We rationally hypothesized that bacterial endotoxin LPS would be one of this natural ligands for three reasons. First, LPS is highly toxic and must be rapidly eliminated from host circulation, which is performed mainly by LSECs scavenger receptors of unknown identity.[10, 18] Second, due to its amphiphilic nature, LPS self-assembles into small anionic NPs with a diameter of ~50 nm, resembling synthetic NPs.[36, 37] Third, Stabilin-2 has been shown to bind to Gram-negative

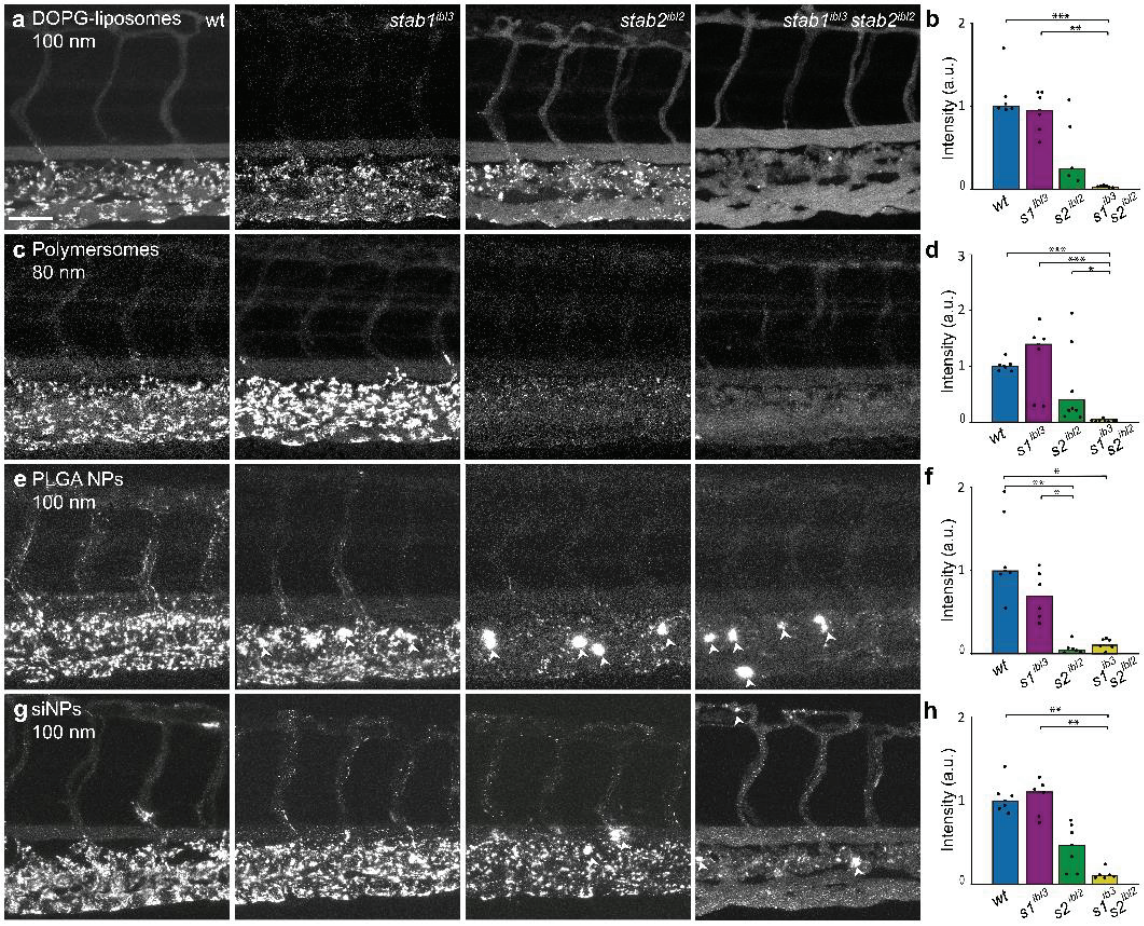

Figure 3. Combined contribution of Stabilin-1 and Stabilin-2 in the clearance of anionic NPs. (a-b) Tissue level view (40x) and quantification of fluorescently labeled DOPG-liposomes, **(c-d)** polymersomes, **(e-f)** PLGA NPs, **(g-h)** siNPs after *i.v.* injection (1 nL) in wt (AB/TL), *stab1*^{ibl3}, *stab2*^{ibl2} single and *stab1*^{ibl3}*stab2*^{ibl2} double mutants at 1-1.5 hours post injection (hpi). White arrows indicate apparent NP uptake within plasma-exposed macrophages. Scale bar: 50 µm. Graphs represent intensity of fluorescent NPs in wt and *stab* mutants. Bar height represents median values, dots are individual data points, and brackets indicate significant values (*P< 0.05, **P<0.01, ***P<0,001) based on Kruskal-Wallis tests followed by two-tailed Dunn's tests with Bonferroni correction.

bacteria - which contain LPS - *in vitro*.[38] To investigate whether circulating LPS is indeed cleared by SECs through Stabilin receptors, fluorescently labeled LPS (Alexa488-LPS) from the Gram-negative bacterium *Salmonella minnesota*[39] was *i.v.* administered. LPS diluted into a salt suspension is proposed to aggregate into micelles at concentrations above the critical micelle concentration (CMC).[36, 37, 40] The LPS concentration injected (500 µg/ml) is above the CMC (~10 µg/ml)[40] even after dilution into the blood of a zebrafish embryo (estimated 30-fold dilution factor, excluding red blood cells, at 2 dpf).[41] Distribution of fluorescent LPS in Tg(*mpeg1:*mCherry) zebrafish, shows no extensive co-localization with labeled macrophages (**Supplementary Figure 5**). This result indicates that phagocytosis by plasma-exposed macrophages does not represent the main clearance route of LPS in the zebrafish embryo, at 56 hpf. Instead, LPS was associated mainly with SECs located in the caudal vein region of wt zebrafish (**Figure 4a,e**), confirming their functional homology to mammalian LSECs.[10]

Next, we injected LPS in *stab2, stab1* and double mutant zebrafish embryos (**Figure 4b-d, f-h**). Association of LPS with SECs was maintained in *stab2* mutants (**Figure 4b, g**). In this case, although a slight decrease in the LPS clearance was observed compared to wt embryos, SEC-uptake was not significantly changed between these two groups (**Figure 4i**). Importantly, LPS uptake by SECs was reduced in *stab1* knockout and completely abrogated in $stab^{DKO}$ mutants, leading to a strong increased level of LPS in circulation (**Figure 4d,h**). This result revealed a cooperative function of Stabilin-1 and Stabilin-2 in LPS uptake and clearance. The loss of LPS uptake in the double knockouts was very similar to that observed after pre-administration of a competitive inhibitor dextran sulfate (**Supplementary Figure 6**), indicating LPS is a common ligand for Stabilin-1 and Stabilin-2, and both receptors are redundantly required for the removal of LPS from the circulation.

3.4 Discussion and Conclusion

The understanding of *in vivo* behavior of NPs and their molecular and cellular interactions after *i.v.* administrations is essential to improve efficacy and pharmacokinetics of nanomaterials. Here, we identify Stabilin-1, a scavenger receptor expressed in LSECs in mammals, is involved in the clearance of small anionic NPs. Interestingly, while mice lacking both *Stab1* and *Stab2* revealed a glomerulofibrotic nephropathy secondary to impaired liver clearance of noxious blood factors[42, 43] leading to strongly reduced viability, we observed that $stab^{DKO}$ adult zebrafish were obtained in mendelian ratios and were phenotypically

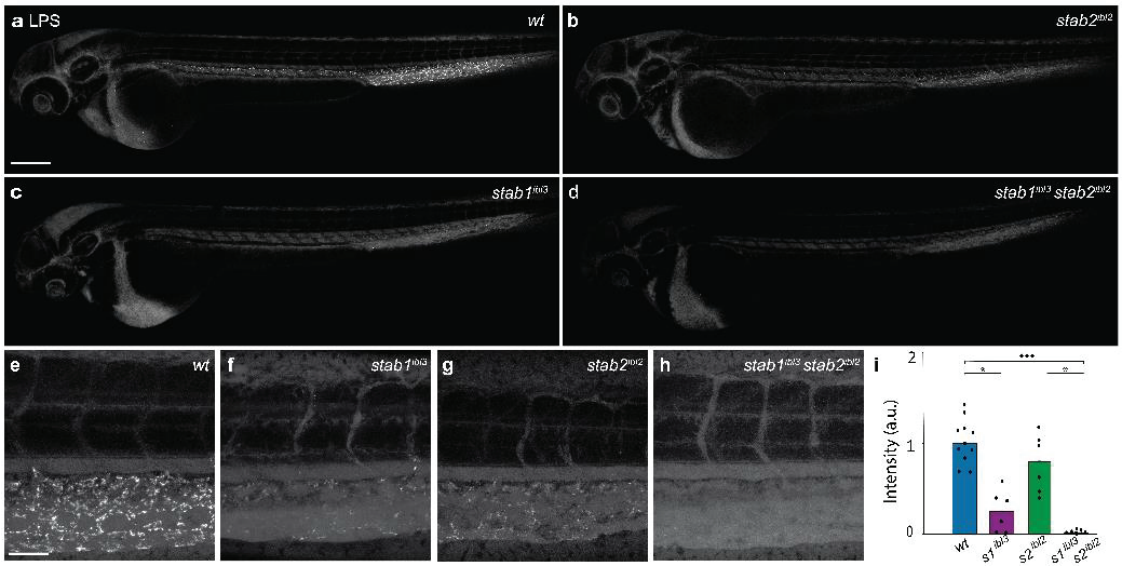

Figure 4. LPS clearance is mediated by Stabilin-1 and Stabilin-2. (a) Biodistribution of Alexa488 LPS (1 nL of 500 µm/mL) in wt (*AB/TL*), **(b)** *stab2*^{ibl2} mutant, **(c)** *stab1*^{ibl3} mutant, **(d)** *stab1*^{ibl3}*stab2*^{ibl2} double mutant at 56 hpf, 1.5 hpi, whole body view (10x). Scale bar: 200 µm. **(e-h)** Tissue level views, caudal region (40x). Scale bar: 50 µm. **(i)** Graph represents intensity of fluorescent LPS in wt and *stab* mutants. Bar height represents median values, dots represent individual data points, and brackets indicate significant values (*P< 0.05, ***P<0,001) based on Kruskal-Wallis tests followed by two-tailed Dunn's tests with Bonferroni correction.

indistinguishable from single mutant and wt zebrafish. Since the reduced viability observed in *Stab1/Stab2* double knockout mice is due mainly to kidney failure, the viability of *stab*^{DKO} fish potentially reflects the high regenerative capacity of the zebrafish kidney.[44]

Through comparison of NP biodistribution in wt and single/double Stabilin mutants we could quantify the relative contribution of Stabilin receptors to the clearance of specific NPs in zebrafish embryos. The analysis of physicochemical properties (**Supplementary Table 3**) and *in vivo* biodistribution of NPs involved in differential uptake for both Stabilin receptors revealed a dependency on size of the particle. Particle size is a critical parameter affecting cellular uptake of nanotherapeutics.[45] Depending on the intended application (*e.g.* drug targeting, vaccine delivery or nucleic acid delivery) an optimal size range is desired.[46, 47] In addition, improved internalization associated with small nanoparticles (~25-50 nm) has been previously shown.[48, 49] Gold nanoparticles in this size range coated with antibodies, for example, display improved endocytosis and regulation of cellular functions.[48] Similarly, ~25-50 nm range has been suggested as an optimal size to reach the maximum cellular uptake.[49] For *in vivo* activity of small

particles, NP clearance by the liver is an important factor influencing biodistribution, but so far has not been linked to a specific receptor. The preference between Stabilin-1 and Stabilin-2 could be attributed indirectly to biological factors or to differences in the structural domains. Biologically, although NP protein corona formation *in vivo* is known to affect the fate of NPs, the different chemistries of the various NPs involved in this study strongly suggest that charge and size are predominant requirements in the interactions between NPs and Stabilin receptors. Structurally, both receptors are initially expressed as a 310 kDa protein, have a very similar domain structure, and are known to share a very common ligand binding profile.[23] So far, it is unknown which structural differences could explain the differential requirement for both receptors to NP clearance.

Besides NPs, the identification of a endogenous ligand of Stabilins, LPS provides important information in the mechanism of clearance of endotoxins. Mechanistically, LPS is known to be detected through toll-like receptor factor 4 and myeloid differentiation factor 2 (TLR4/Md-2) complex in mammals.[50] Inflammatory responses to LPS have been previously observed in the zebrafish,[5] but the signaling involved in LPS-sensing is not well understood. Since SECs in the zebrafish are functionally homologous to LSECs[15] and LPS is known to be recognized by LSECs in mammals,[10, 18] we believe our results contribute to the mechanistic understanding of recognition and clearance of endotoxin LPS – especially at high concentrations above the CMC - important not only in the identification and study of host-pathogen interactions but also in inflammation and immunity responses.

In conclusion, by using the zebrafish as model that allows genetic analysis and imaging of NP clearance *in vivo*, we demonstrate that Stabilin-1 is required independently of Stabilin-2, for endothelial clearance of small anionic Qdots, CCMV-VLP, SCNPs (6-30 nm) from the circulation. Since NPs with very different chemistries are cleared by Stabilin-1, this strongly suggests negative surface charge and size as the predominant factors that determine a requirement for Stabilin-1 in NP clearance. We also show a combined contribution between Stabilin-1 and Stabilin-2 in the clearance of anionic liposomes, polymeric PS and siNPs (~100 nm) and in the removal of LPS. These results reveal a partial redundancy between *stab1* and *stab2*, both important for NPs clearance, and suggest a differential uptake where size is one of the key parameters determining the selective uptake by each receptor. Given size is particularly important in vaccine development, biomedical imaging applications and delivery technologies, improved mechanistic insights into the interactions between size-

selected NPs and the liver at the molecular level contributes to the optimization of small nanomaterials and avenues for receptor-specific targeting.

3.5 Materials and Methods

Nanoparticles

Fluorescent Alexa488-LPS from *Salmonella minnessota,* PS NPs, and Qdots layered with an organic CdSeS/ZnS and a carboxylic acid as a reactive group (consisting of a monolayer of octylamine-modified poly acrylic acid and a monolayer of poly acrylic acid -PnOAm-co-PAA- copolymer cap), were purchased from Life Technologies (Eugene, US) by Thermo Fisher Scientific and Sigma-Aldrich (The Netherlands). SiNPs were purchased from HiQ-Nano SRL (Arnesano, Italy). FluoHA was prepared through conjugation of hyaluronic acid (100 kDa) with fluorescein isothiocyanate (Isomer I, Sigma-Aldrich The Netherlands) as previously described.[51] PLGA NPs were formulated in house with a microfluidic system. DOPG-liposomes containing 1 mol% DOPE-lissamine rhodamine were formulated with a extrusion system as described previously.[15] Negatively charged SCNPs were synthesized, characterized and provided by our collaborators N. Hamelmann and J. Paulusse. (University of Twente, The Netherlands). Rhodamine-loaded polymersomes[31] on PIB/PEG block copolymers were a kind gift from S. Askes & S. Bonnet (Leiden University, The Netherlands). Atto-647 labeled CCMV-VLPs[29] were a kind gift from R. van der Hee & J. Cornelissen (University of Twente, The Netherlands).

Zebrafish handling and strains

Zebrafish (*Danio rerio*) were maintained and handled according to the guidelines from the Zebrafish Model Organism Database (http://zfin.org) and in compliance with the directives of the local animal welfare committee of Leiden University. Housing and husbandry recommendations were followed as recommended by Alestrom *et al*.[52] Fertilization was performed by natural spawning at the beginning of the light period and eggs were raised at 28.5°C in egg water (60 µg/ml Instant Ocean sea salts). The following established zebrafish strains were used in this study: Tg(*mpeg1:*mCherry),[53] Tg(*flt1*^{enh}*:*RFP)^{hu5333},[54] Tg(*flt4*^{BAC}*:*YFP)^{hu7135},[55] *stab2*^{ibl2},[15] *stab1*^{ibl3} (described in this work).

CRISPR/Cas9 mutagenesis

Cloning-free sgRNAs for CRISPR/Cas9 mutagenesis were designed and synthesized as described.[56, 57] 125 pg of sgRNA (**Supplementary Table 2**) and 300 pg cas9 mRNA were co-injected into a single-cell wt embryo fish. Primers nucleotide sequences, sgRNA sequence and predicted *stab1* and *stab2* amino acid sequences in the *stab1*^{ibl3} and *stab2*^{ibl2} were used as reported.[15] Double *stab1*^{ibl3} and *stab2*^{ibl2} mutants were generated by crossing adult homozygous zebrafish *stab2*^{ibl2} and *stab* ^{ibl3} mutants.

In situ hybridization

Whole-mount ISH was performed as described previously.[58] The sequences for probes generation (*stab1*, *stab*2, *mrc1)* were used as reported.[15]

Zebrafish i.v. microinjections and imaging

NPs formulation were injected into 2-day old zebrafish embryos (52-56 hpf) using a modified microangraphy protocol.[59] One nl volume of NP formulation were calibrated and injected into the duct of Cuvier after embryos were embedded in 0.4% agarose containing 0.01% tricaine as described.[15] We created a small injection space by penetrating the skin with the injection microneedle and gently pulling the needle back, thereby creating a small pyramidal space in which the NPs were injected. Representative embryos were randomly selected according to successful injections and imaged by confocal microscopy after one hour post injection. Confocal z-stacks were captured on a Leica TCS SPE or LEICA TCS SP8 confocal microscope, using a 10x air objective (HCX PL FLUOTAR), a 40x water-immersion objective (HCX APO L), or a 63x oil-immersion objective (HC PL APO CS). In order to compare images between strains, microscopy settings (laser intensity, gain and offset) were identical between stacks and sessions. Whole-embryo images were a compilation of 3-4 overlapping z-stacks. Fiji distribution of ImageJ[60, 61] was used to process and quantify images. At least 6 images were used for quantification.

Imaging quantification

Quantification was performed in the caudal region of the zebrafish, a region known to contain Stabilin endothelium, and that includes the dorsal aorta, the caudal vein and the caudal hematopoietic tissue (could include macrophages associated with SECs). First, an average intravascular within the dorsal aorta was

measured within a rectangular area in a single confocal slice that captured the center of the dorsal aorta. This measurement was repeated three times per embryo in independent sites within the dorsal aorta. Next, the maximum intensity value obtained per image was used to adjust the threshold according to the max value measure in the aorta (in circulation), generating a binary image. The strong fluorescence signal observed by accumulated phagocytosed NPs could lead to a misinterpretation of a SEC signal. For that reason and since the aim of this quantification is to compare the contribution of stabilins in the clearance of NPs and not directly the phagocytosis of macrophages, we attempt to remove the signal potentially associated with macrophages by means of size filtering (0,25-20 um) and to use a qualitative approach to refer to macrophages uptake. From the resulting image, a value of 254 was subtracted in order to get values of 0 (no signal) or 1 (fluorescence). The image of interest was multiplied (max x mask) and to obtain the mean intensity and the area (%) of the analyzed image. Having these values, the total area with signal (% area x and total signal /100) and the total signal (mean signal x total area) were calculated. The median intensity value of the total signal obtained from the mutants was normalized against the wt counterpart. The angle of the dorsal aspect of the dorsal aorta (a straight line) was measured and then concatenated. Images were rotated to orient the DA horizontally within the image and were subsequently cropped.

Statistical analysis

For comparisons between multiple groups, we used Kruskal-Wallis tests followed by two-tailed Dunn's tests with Bonferroni correction using the PMCMR package in R or GraphPad Prism. No statistical methods were used to predetermine sample size, but group sizes were greater than 5 in order for the null distribution of the Kruskal-Wallis statistic to approximate the X^2 distribution (with k-1 degrees of freedom). Graphs show all individual data points and the median. Confocal image stacks (raw data) are available upon request.

3.6 Abbreviations

CCMV-VLP	cowpea chlorotic mottle virus derived virus-like particles
dpf	day(s) post fertilization
DOPG	1,2-dioleoyl-*sn*-glycero-3-phospho-(1'-*rac*-glycerol)
ECs	endothelial cells
fluoHA	fluorescently labeled hyaluronic acid
hpi	hour(s) post injection
ISH	*in situ* hybridization
KCs	kupffer cells
LPS	lipopolysaccharide
LSECs	liver sinusoidal endothelial cells
NP	nanoparticle(s)
PIB-PEG	polyisobutylene-polyethylene glycol
PLGA	poly(D,L-lactide-co-glycolide
PS	polystyrene
Qdots	quantum dots
SCNPs	single chain nanoparticles
SECs	scavenging endothelial cells
siNPs	silica nanoparticles
wt	wildtype

3.7 Supporting Information

Supplementary Table 1. Scavenger receptors RNA expression in mouse liver. Comparison of gene expression according to 3 published single-cell RNA sequencing datasets. Values are calculated through dividing the average RNA count over all LSECs for the respective scavenger receptor gene by the average RNA count over all LSECs of all scavenger receptors. The colors indicate the most abundant scavenger receptors expressed in LSECs, consistent in the 3 datasets, from light yellow to red (higher relative expression of one scavenger receptor over all others).

SR family	Gene	Halpern et al.[25]	Tabula Muris[27]	Sabbagh et al.[26]
SR-A1	*Msr1*	1.01	0.71	0.69
SR-A3	*Scara3*	0.00	0.00	0.00
SR-A4	*Colec12*	0.13	0.03	0.05
SR-A5	*Scara5*	0.00	0.00	0.00
SR-A6	*Marco*	0.09	0.00	0.00
SR-B1	*Scarb1*	0.38	0.41	0.24
SR-B2	*Cd36*	0.74	1.91	2.54
SR-D1	*Cd68*	0.09	0.02	0.01
SR-E1	*Olr1*	0.00	0.00	0.01
SR-E2	*Clec7a*	0.13	0.01	0.00
SR-E3	*Mrc1*	9.68	8.14	3.93
SR-E4	*Asgr1*	0.33	0.01	0.00
SR-F1	*Scarf1*	0.50	0.56	0.10
SR-F2	*Scarf2*	0.00	0.00	0.00
SR-F3	*Megf10*	0.00	0.00	0.00
SR-G1	*Cxcl16*	1.08	1.18	0.12
SR-H1	*Stab1*	3.62	3.71	4.10
SR-H2	*Stab2*	5.58	7.27	12.18
SR-I1	*Cd163*	0.12	0.01	0.00
SR-I2	*Cd163l*	0.00	0.00	0.00
SR-J1	*Ager*	0.00	0.00	0.01
SR-K1	*Cd44*	0.26	0.00	0.00
SR-L1	*Lrp1*	0.27	0.02	0.02
SR-L2	*Lrp2*	0.00	0.00	0.00

Supplementary Table 2. Guide RNA sequence for CRISPR/Cas and forward and reverse primers of *stab1* mutant (-1nt).[15] Target sequence in green.

Stab1	Sequence
sgRNA	TAATACGACTCACTATAGGTAG**AAATTGGCGGTCGCC**GTTTTAGAGCTAGAAATAGC
Primer Forward	TGTAAAACGACGGCCAGTAGACTTTGGGTGCTGTAACCAT
Primer Reverse	GTGTCTTCCTAACGTACATTTGAACCCGT

Supplementary Table 3. Physicochemical properties of NPs used.

NPs	Concentration Injected	Size (nm) ^	PDI	ζ-potential (mV) ^	Reference
Carboxylated QDots	0.25 mg/mL	6 *	ND	-70.8	*
Polymersomes PIB:PEG(1:0.75 mol/ratio)	1 mg/mL	73.34	0.181	-24.0	[62]
DOPG-liposomes	1 mM (total lipids) + 1 mol% DOPE-LR	112.1	0.042	-37.0	[15]
CCMV-VLP T=3 capsids	ND	28	ND	-15.0	[29]**
SCNPs	5 mg/mL	10.0	0.016	-33.0	[30]#
PLGA NPs	0,25 mg/mL	108.0	0.086	-37.1	NA
siNPs 90 nm	10 mg/mL	130.4	0.172	-22.0	*
PS 40 nm 5% solid	0.1 mg/mL	57.3	0.176	-30.7	*
PS 100 nm 2% solid	0.1 mg/mL	107.3	0.022	-51.5	*
PS 200 nm 2 % solid	0.2 mg/mL	246.3	0.090	-51.0	*
PS 500 nm 2 % solid	0.4 mg/mL	553.8	0.339	-46.8	*
PS 1000 nm 2% solid	2 mg/mL	1191.8	0.628	-74.7	*
PS 2000 nm 2% solid	10 mg/mL	1474.0	0.128	-40.1	*

^Measurements were performed in technical triplicates.
PDI: polydispersity index. ND: Not determined. NA: Not applicable. LR: Lissamine rhodamine.
*Commercially available.
** Unmodified (no conjugated dye).
# Anionic SCNPs (DTAF labeled, not included in ref [9]).

Size and zeta potentials measurements

The formulations were analyzed at room temperature in ddH_2Oon a Malvern Zetasizer Nano ZS (Malvern Panalytical B.V., Almelo, the Netherlands) to determine the hydrodynamic particles sizes and polydispersity indexes (PDIs)

with dynamic light scattering (measured at a detection angle of 174.7°), and the zeta potentials with laser Doppler electrophoresis. Before the measurements, the formulations were diluted. The measurements were performed in technical triplicates and the average was reported.

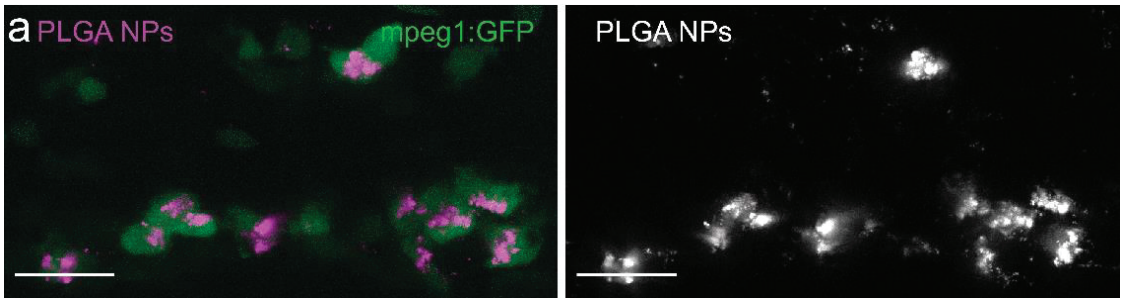

Supplementary Figure 1. Nanoparticles phagocytosed by plasma-exposed macrophages. (a) Colocalization of PLGA NPs (magenta) in *stab*^{DKO} zebrafish Tg(*mpeg1*:mCherry) stably expressing GFP in macrophages at 1.5 hpi. Scale bars: 25 µm.

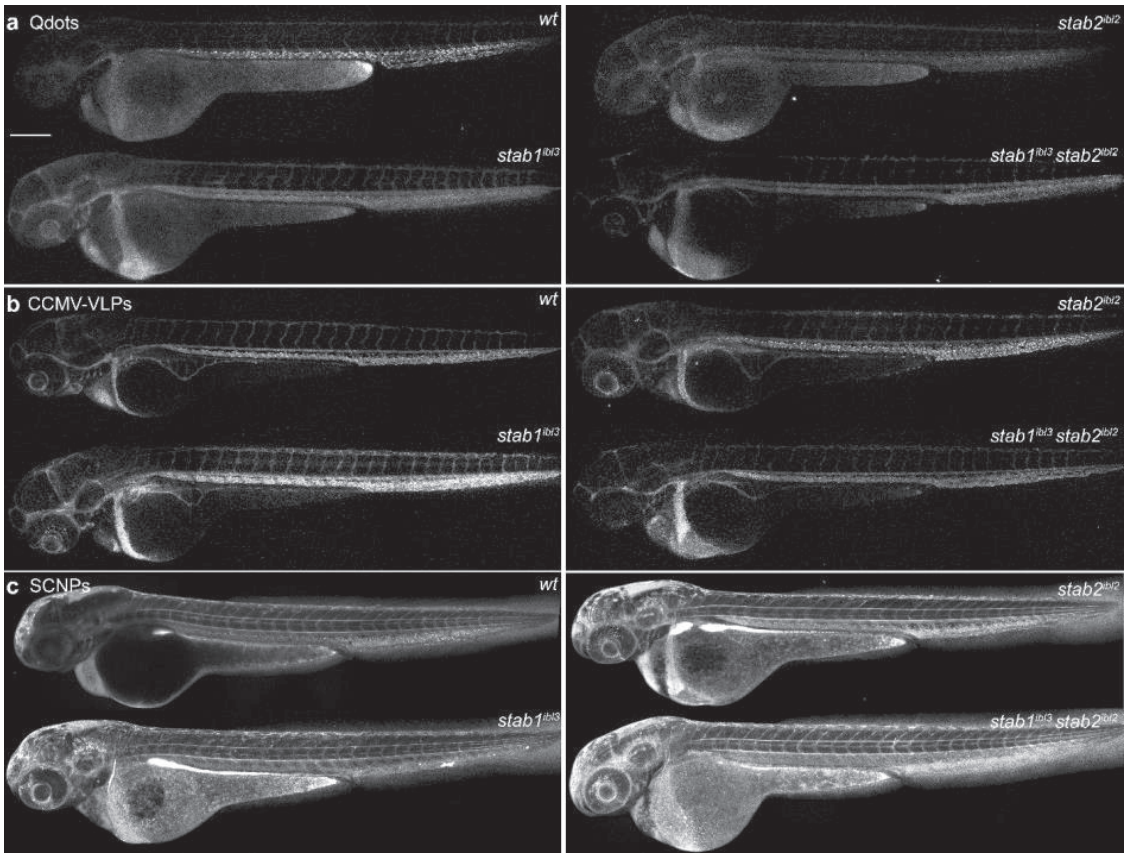

Supplementary Figure 2. Anionic NPs cleared mainly by Stabilin-1 receptor. (a) Biodistribution and uptake of Qdots, **(b)** CCMV-VLPs, and **(c)** SCNPs in whole zebrafish view of wildtype (*AB/TL*), *stab1*^{ibl3}, *stab2*^{ibl2} single mutants and *stab1*^{ibl3} *stab2*^{ibl2} double mutants at 56 hpf,1-1.5 hpi. Scale bar 200 µm.

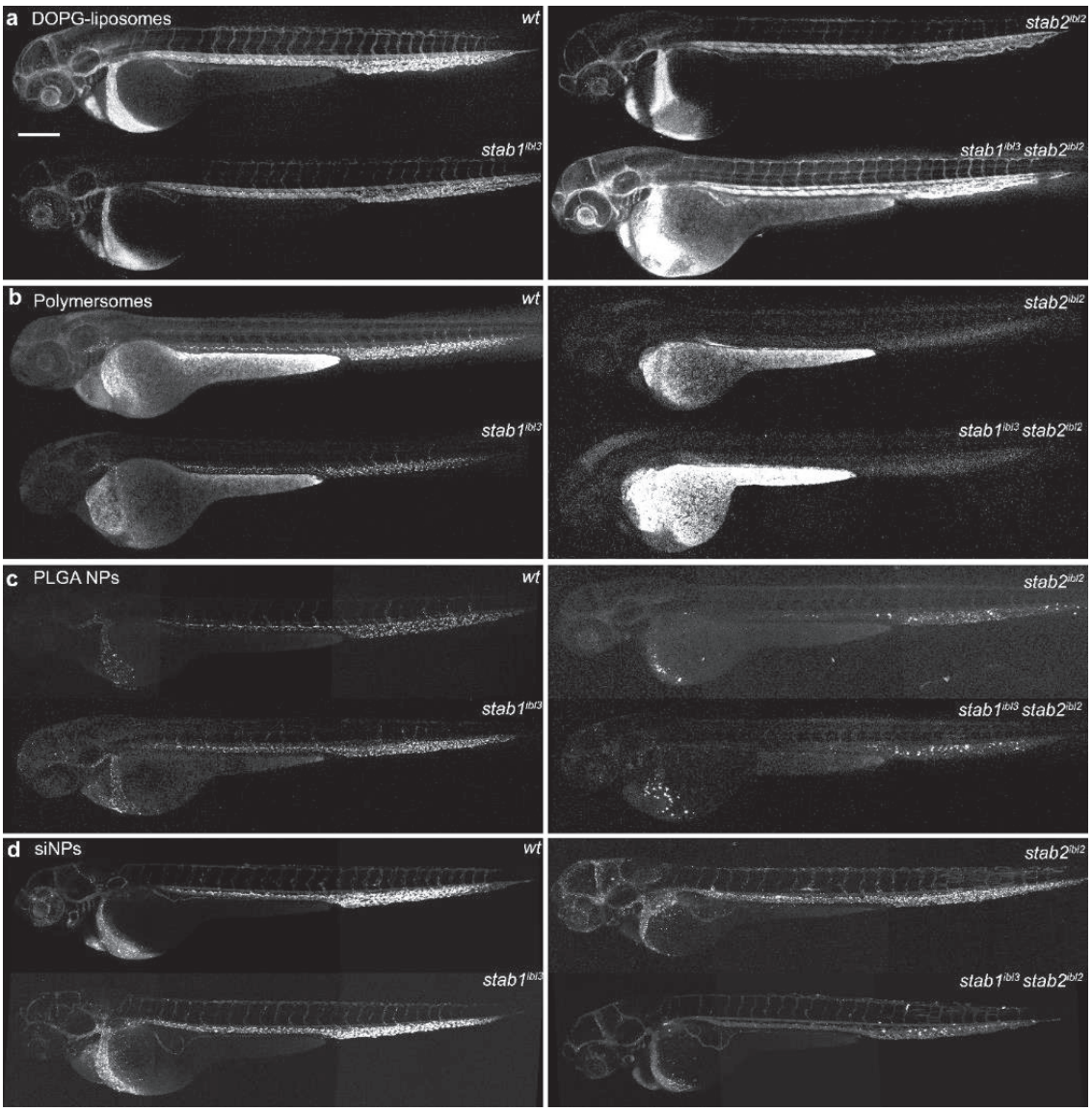

Supplementary Figure 3. Anionic NPs cleared by Stabilin-1 and/or Stabilin-2 receptors. (a) Biodistribution and uptake of DOPG-liposomes, **(b)** Polymersomes **(c)** PLGA NPs, **(d)** siNPs in wildtype (*AB/TL*), *stab1*^{ibl3}, *stab2*^{ibl2} single mutants and *stab1*^{ibl3} *stab2*^{ibl2} double mutants at 56 hpf,1-1.5 hpi. Scale bar 200 μm.

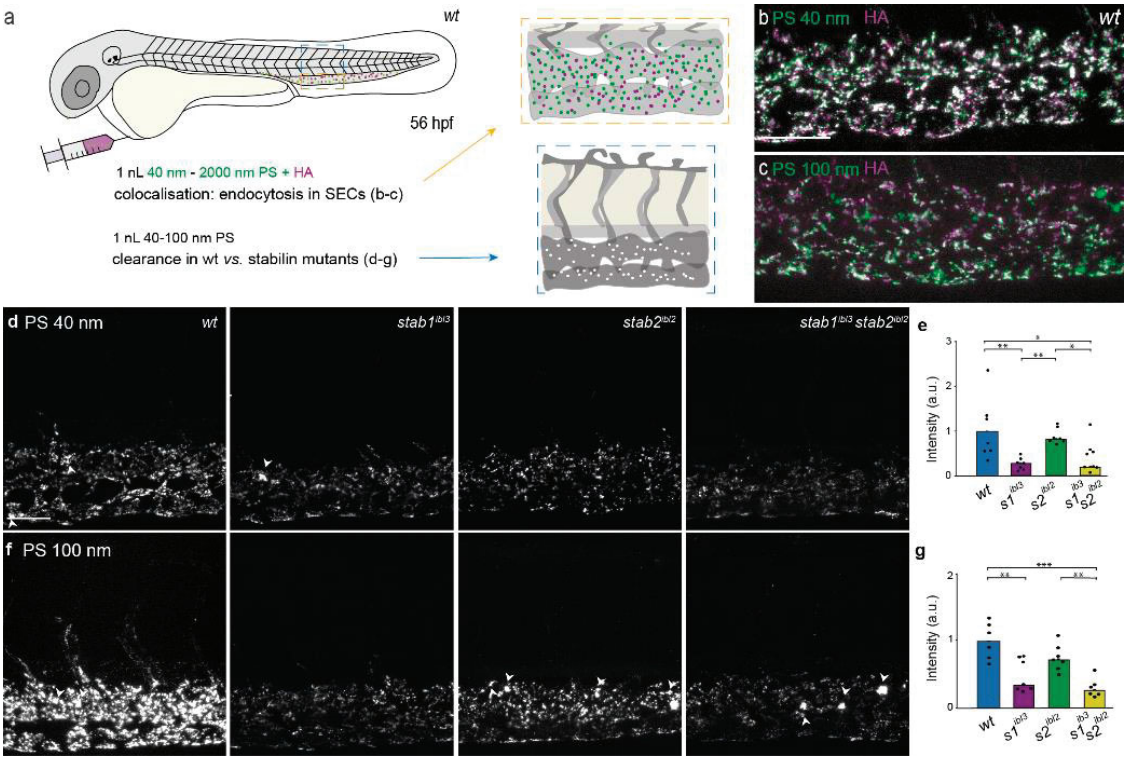

Supplementary Figure 4. Uptake of PS particles by SECs through Stabilin-1 and/or Stabilin-2. (a) Schematic representation of a zebrafish embryo and the injection site at 2 days old (54-56 hpf). Boxes shows the region imaged. **(b-c)** Distribution and endocytosis of PS, in green, with a size of 40, and 100 respectively, co-injected with fluoHA (20 mg/mL) (in magenta) in wt zebrafish at 1-1.5 hpi. FluoHA was used as an *in vivo* marker for SECs, colocalization of fluoHA with PS indicates endocytosis. **(d-g)** Uptake and images quantification of 40 nm and 100 nm PS particles (1 nL of 100 µg/mL) in wt, and *stabilin* mutants at 1-1.5 hpi. White arrows indicate apparent PS uptake in blood resident macrophages. Scale bars: 50 µm. Bar height represents median values, dots represent individual data points, and brackets indicate significant values (*P< 0.05, **P<0.01, ***P<0,001) based on Kruskal-Wallis tests followed by two-tailed Dunn's tests with Bonferroni correction.

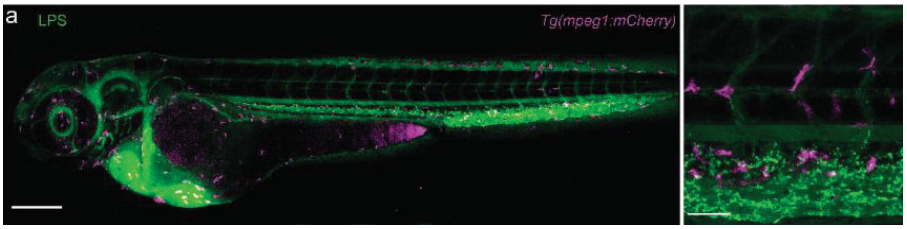

Supplementary Figure 5. Distribution of fluorescently labeled LPS. (a) Alexa488-LPS in Tg(*mpeg1*:mCherry) zebrafish stably expressing mCherry in macrophages at 1.5 hpi. Scale bars: 200 µm (whole body view) and 50 µm (tissue level view).

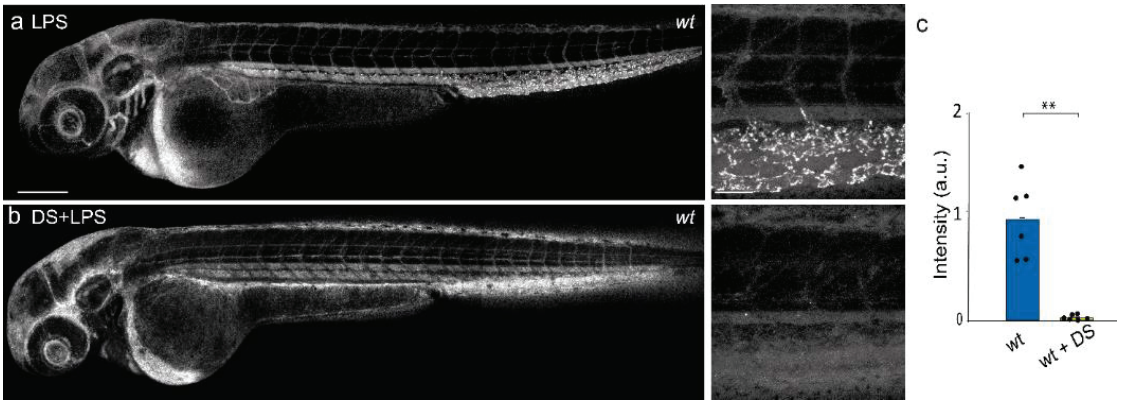

Supplementary Figure 6. Dextran sulfate (DS) inhibits uptake of LPS by SECs. (a) Biodistribution of Alexa488 LPS in wildtype (*AB/TL*) **(b)** LPS biodistribution after 30 min of dextran sulfate (20 mg/mL) at 56 hpf, 1.5 hpi, whole body view and respective tissue level view (caudal region). Scale bar: 200 µm (whole view) and 50 µm (tissue level). **(c)** Graph represents intensity of fluorescent LPS in wt and after administration of dextran sulfate, DS. Bar height represents median values, dots represent individual data points, and brackets indicate significant value (**P<0.01) based on Kruskal-Wallis tests followed by two-tailed Dunn's tests with Bonferroni correction using the PMCMR package in R.

3.9 References

1. Zhang, Y. N.; Poon, W.; Tavares, A. J.; McGilvray, I. D.; Chan, W. C. W., Nanoparticle-liver interactions: Cellular uptake and hepatobiliary elimination. *J Control Release* **2016,** *240*, 332-348.
2. Polo, E.; Collado, M.; Pelaz, B.; Del Pino, P., Advances toward More Efficient Targeted Delivery of Nanoparticles in Vivo: Understanding Interactions between Nanoparticles and Cells. *ACS Nano* **2017,** *11* (3), 2397-2402.
3. Choi, H. S.; Liu, W.; Misra, P.; Tanaka, E.; Zimmer, J. P.; Itty Ipe, B.; Bawendi, M. G.; Frangioni, J. V., Renal clearance of quantum dots. *Nat Biotechnol* **2007,** *25* (10), 1165-1170.
4. Tsoi, K. M.; MacParland, S. A.; Ma, X. Z.; Spetzler, V. N.; Echeverri, J.; Ouyang, B.; Fadel, S. M.; Sykes, E. A.; Goldaracena, N.; Kaths, J. M.; Conneely, J. B.; Alman, B. A.; Selzner, M.; Ostrowski, M. A.; Adeyi, O. A.; Zilman, A.; McGilvray, I. D.; Chan, W. C., Mechanism of hard-nanomaterial clearance by the liver. *Nat Mater* **2016,** *15* (11), 1212-1221.
5. Hayashi, Y.; Takamiya, M.; Jensen, P. B.; Ojea-Jimenez, I.; Claude, H.; Antony, C.; Kjaer-Sorensen, K.; Grabher, C.; Boesen, T.; Gilliland, D.; Oxvig, C.; Strahle, U.; Weiss, C., Differential Nanoparticle Sequestration by Macrophages and Scavenger Endothelial Cells Visualized in Vivo in Real-Time and at Ultrastructural Resolution. *ACS Nano* **2020,** *14* (2), 1665-1681.
6. Shiratori, Y.; Tananka, M.; Kawase, T.; Shiina, S.; Komatsu, Y.; Omata, M., Quantification of sinusoidal cell function in vivo. *Semin Liver Dis* **1993,** *13* (1), 39-49.
7. Tenzer, S.; Docter, D.; Kuharev, J.; Musyanovych, A.; Fetz, V.; Hecht, R.; Schlenk, F.; Fischer, D.; Kiouptsi, K.; Reinhardt, C.; Landfester, K.; Schild, H.; Maskos, M.; Knauer, S. K.; Stauber, R. H., Rapid formation of plasma protein corona critically affects nanoparticle pathophysiology. *Nat Nanotechnol* **2013,** *8* (10), 772-781.
8. Rejman, J.; Oberle, V.; Zuhorn, I. S.; Hoekstra, D., Size-dependent internalization of particles via the pathways of clathrin- and caveolae-mediated endocytosis. *Biochem J* **2004,** *377* (Pt 1), 159-169.
9. Breiner, K. M.; Schaller, H.; Knolle, P. A., Endothelial cell-mediated uptake of a hepatitis B virus: a new concept of liver targeting of hepatotropic microorganisms. *Hepatology* **2001,** *34* (4 Pt 1), 803-808.
10. Yao, Z.; Mates, J. M.; Cheplowitz, A. M.; Hammer, L. P.; Maiseyeu, A.; Phillips, G. S.; Wewers, M. D.; Rajaram, M. V.; Robinson, J. M.; Anderson, C. L.; Ganesan, L. P., Blood-Borne Lipopolysaccharide Is Rapidly Eliminated by Liver Sinusoidal Endothelial Cells via High-Density Lipoprotein. *J Immunol* **2016,** *197* (6), 2390-2399.
11. van Oosten, M.; van de Bilt, E.; van Berkel, T. J.; Kuiper, J., New scavenger receptor-like receptors for the binding of lipopolysaccharide to liver endothelial and Kupffer cells. *Infect Immun* **1998,** *66* (11), 5107-5112.
12. Li, R.; Oteiza, A.; Sorensen, K. K.; McCourt, P.; Olsen, R.; Smedsrod, B.; Svistounov, D., Role of liver sinusoidal endothelial cells and stabilins in elimination of oxidized low-density lipoproteins. *Am J Physiol Gastrointest Liver Physiol* **2011,** *300* (1), G71-81.
13. Wohlleber, D.; Knolle, P. A., The role of liver sinusoidal cells in local hepatic immune surveillance. *Clin Transl Immunology* **2016,** *5* (12), e117.
14. Sellaro, T. L.; Ravindra, A. K.; Stolz, D. B.; Badylak, S. F., Maintenance of hepatic sinusoidal endothelial cell phenotype in vitro using organ-specific extracellular matrix scaffolds. *Tissue Eng* **2007,** *13* (9), 2301-2310.
15. Campbell, F.; Bos, F. L.; Sieber, S.; Arias-Alpizar, G.; Koch, B. E.; Huwyler, J.; Kros, A.; Bussmann, J., Directing Nanoparticle Biodistribution through Evasion and Exploitation of Stab2-Dependent Nanoparticle Uptake. *ACS Nano* **2018,** *12* (3), 2138-2150.
16. Seternes, T.; Sorensen, K.; Smedsrod, B., Scavenger endothelial cells of vertebrates: a nonperipheral leukocyte system for high-capacity elimination of waste macromolecules. *Proc Natl Acad Sci U S A* **2002,** *99* (11), 7594-7597.
17. Wong, K. S.; Proulx, K.; Rost, M. S.; Sumanas, S., Identification of vasculature-specific genes by microarray analysis of Etsrp/Etv2 overexpressing zebrafish embryos. *Dev Dyn* **2009,** *238* (7), 1836-1850.
18. Hampton, R. Y.; Golenbock, D. T.; Penman, M.; Krieger, M.; Raetz, C. R., Recognition and plasma clearance of endotoxin by scavenger receptors. *Nature* **1991,** *352* (6333), 342-344.

19. Verweij, F. J.; Revenu, C.; Arras, G.; Dingli, F.; Loew, D.; Pegtel, D. M.; Follain, G.; Allio, G.; Goetz, J. G.; Zimmermann, P.; Herbomel, P.; Del Bene, F.; Raposo, G.; van Niel, G., Live Tracking of Inter-organ Communication by Endogenous Exosomes In Vivo. *Dev Cell* **2019,** *48* (4), 573-589 e574.
20. Park, S. Y.; Jung, M. Y.; Kim, H. J.; Lee, S. J.; Kim, S. Y.; Lee, B. H.; Kwon, T. H.; Park, R. W.; Kim, I. S., Rapid cell corpse clearance by stabilin-2, a membrane phosphatidylserine receptor. *Cell Death Differ* **2008,** *15* (1), 192-201.
21. Miller, C. M.; Donner, A. J.; Blank, E. E.; Egger, A. W.; Kellar, B. M.; Ostergaard, M. E.; Seth, P. P.; Harris, E. N., Stabilin-1 and Stabilin-2 are specific receptors for the cellular internalization of phosphorothioate-modified antisense oligonucleotides (ASOs) in the liver. *Nucleic Acids Res* **2016,** *44* (6), 2782-2794.
22. Alidori, S.; Bowman, R. L.; Yarilin, D.; Romin, Y.; Barlas, A.; Mulvey, J. J.; Fujisawa, S.; Xu, K.; Ruggiero, A.; Riabov, V.; Thorek, D. L.; Ulmert, H. D.; Brea, E. J.; Behling, K.; Kzhyshkowska, J.; Manova-Todorova, K.; Scheinberg, D. A.; McDevitt, M. R., Deconvoluting hepatic processing of carbon nanotubes. *Nat Commun* **2016,** *7*, 12343.
23. Harris, E. N.; Cabral, F., Ligand Binding and Signaling of HARE/Stabilin-2. *Biomolecules* **2019,** *9* (7), 273.
24. Nowak, M. A.; Boerlijst, M. C.; Cooke, J.; Smith, J. M., Evolution of genetic redundancy. *Nature* **1997,** *388* (6638), 167-171.
25. Halpern, K. B.; Shenhav, R.; Massalha, H.; Toth, B.; Egozi, A.; Massasa, E. E.; Medgalia, C.; David, E.; Giladi, A.; Moor, A. E.; Porat, Z.; Amit, I.; Itzkovitz, S., Paired-cell sequencing enables spatial gene expression mapping of liver endothelial cells. *Nat Biotechnol* **2018,** *36* (10), 962-970.
26. Sabbagh, M. F.; Heng, J. S.; Luo, C.; Castanon, R. G.; Nery, J. R.; Rattner, A.; Goff, L. A.; Ecker, J. R.; Nathans, J., Transcriptional and epigenomic landscapes of CNS and non-CNS vascular endothelial cells. *Elife* **2018,** *7*.
27. Schaum, N.; Karkanias, J.; Neff, N. F.; May, A. P.; Quake, S. R.; Wyss-Coray, T.; Darmanis, S.; Batson, J.; Botvinnik, O.; Chen, M. B., et al., Single-cell transcriptomics of 20 mouse organs creates a Tabula Muris. *Nature* **2018,** *562* (7727), 367-372.
28. Stoll, S. J.; Bartsch, S.; Kroll, J., HOXC9 regulates formation of parachordal lymphangioplasts and the thoracic duct in zebrafish via stabilin 2. *PLoS One* **2013,** *8* (3), e58311.
29. Verwegen, M.; Cornelissen, J. J., Clustered nanocarriers: the effect of size on the clustering of CCMV virus-like particles with soft macromolecules. *Macromol Biosci* **2015,** *15* (1), 98-110.
30. Kroger, A. P. P.; Hamelmann, N. M.; Juan, A.; Lindhoud, S.; Paulusse, J. M. J., Biocompatible Single-Chain Polymer Nanoparticles for Drug Delivery-A Dual Approach. *ACS Appl Mater Interfaces* **2018,** *10* (37), 30946-30951.
31. Askes, S. H.; Pomp, W.; Hopkins, S. L.; Kros, A.; Wu, S.; Schmidt, T.; Bonnet, S., Imaging Upconverting Polymersomes in Cancer Cells: Biocompatible Antioxidants Brighten Triplet-Triplet Annihilation Upconversion. *Small* **2016,** *12* (40), 5579-5590.
32. Saez Talens, V.; Arias-Alpizar, G.; Makurat, D. M. M.; Davis, J.; Bussmann, J.; Kros, A.; Kieltyka, R. E., Stab2-Mediated Clearance of Supramolecular Polymer Nanoparticles in Zebrafish Embryos. *Biomacromolecules* **2020,** *21* (3), 1060-1068.
33. Davis, M. E.; Chen, Z. G.; Shin, D. M., Nanoparticle therapeutics: an emerging treatment modality for cancer. *Nat Rev Drug Discov* **2008,** *7* (9), 771-782.
34. Rezvantalab, S.; Drude, N. I.; Moraveji, M. K.; Güvener, N.; Koons, E. K.; Shi, Y.; Lammers, T.; Kiessling, F., PLGA-Based Nanoparticles in Cancer Treatment. *Frontiers in Pharmacology* **2018,** *9* (1260).
35. Raetz, C. R.; Whitfield, C., Lipopolysaccharide endotoxins. *Annu Rev Biochem* **2002,** *71*, 635-700.
36. Sasaki, H.; White, S. H., Aggregation behavior of an ultra-pure lipopolysaccharide that stimulates TLR-4 receptors. *Biophys J* **2008,** *95* (2), 986-993.
37. Wang, C.; Nelson, T.; Chen, D.; Ellis, J. C.; Abbott, N. L., Understanding lipopolysaccharide aggregation and its influence on activation of Factor C. *J Colloid Interface Sci* **2019,** *552*, 540-553.
38. Adachi, H.; Tsujimoto, M., FEEL-1, a novel scavenger receptor with in vitro bacteria-binding and angiogenesis-modulating activities. *J Biol Chem* **2002,** *277* (37), 34264-34270.
39. Triantafilou, K.; Triantafilou, M.; Fernandez, N., Lipopolysaccharide (LPS) labeled with Alexa 488 hydrazide as a novel probe for LPS binding studies. *Cytometry* **2000,** *41* (4), 316-320.
40. Aurell, C. A.; Wistrom, A. O., Critical aggregation concentrations of gram-negative bacterial lipopolysaccharides (LPS). *Biochem Biophys Res Commun* **1998,** *253* (1), 119-123.

41. Craig, M. P.; Gilday, S. D.; Dabiri, D.; Hove, J. R., An optimized method for delivering flow tracer particles to intravital fluid environments in the developing zebrafish. *Zebrafish* **2012,** *9* (3), 108-119.
42. Palani, S.; Elima, K.; Ekholm, E.; Jalkanen, S.; Salmi, M., Monocyte Stabilin-1 Suppresses the Activation of Th1 Lymphocytes. *J Immunol* **2016,** *196* (1), 115-123.
43. Schledzewski, K.; Geraud, C.; Arnold, B.; Wang, S.; Grone, H. J.; Kempf, T.; Wollert, K. C.; Straub, B. K.; Schirmacher, P.; Demory, A.; Schonhaber, H.; Gratchev, A.; Dietz, L.; Thierse, H. J.; Kzhyshkowska, J.; Goerdt, S., Deficiency of liver sinusoidal scavenger receptors stabilin-1 and -2 in mice causes glomerulofibrotic nephropathy via impaired hepatic clearance of noxious blood factors. *J Clin Invest* **2011,** *121* (2), 703-714.
44. Diep, C. Q.; Ma, D.; Deo, R. C.; Holm, T. M.; Naylor, R. W.; Arora, N.; Wingert, R. A.; Bollig, F.; Djordjevic, G.; Lichman, B.; Zhu, H.; Ikenaga, T.; Ono, F.; Englert, C.; Cowan, C. A.; Hukriede, N. A.; Handin, R. I.; Davidson, A. J., Identification of adult nephron progenitors capable of kidney regeneration in zebrafish. *Nature* **2011,** *470* (7332), 95-100.
45. Hoshyar, N.; Gray, S.; Han, H.; Bao, G., The effect of nanoparticle size on in vivo pharmacokinetics and cellular interaction. *Nanomedicine (Lond)* **2016,** *11* (6), 673-692.
46. Hassett, K. J.; Benenato, K. E.; Jacquinet, E.; Lee, A.; Woods, A.; Yuzhakov, O.; Himansu, S.; Deterling, J.; Geilich, B. M.; Ketova, T.; Mihai, C.; Lynn, A.; McFadyen, I.; Moore, M. J.; Senn, J. J.; Stanton, M. G.; Almarsson, O.; Ciaramella, G.; Brito, L. A., Optimization of Lipid Nanoparticles for Intramuscular Administration of mRNA Vaccines. *Mol Ther Nucleic Acids* **2019,** *15*, 1-11.
47. Sykes, E. A.; Chen, J.; Zheng, G.; Chan, W. C., Investigating the impact of nanoparticle size on active and passive tumor targeting efficiency. *ACS Nano* **2014,** *8* (6), 5696-5706.
48. Jiang, W.; Kim, B. Y.; Rutka, J. T.; Chan, W. C., Nanoparticle-mediated cellular response is size-dependent. *Nat Nanotechnol* **2008,** *3* (3), 145-150.
49. Zhang, S.; Li, J.; Lykotrafitis, G.; Bao, G.; Suresh, S., Size-Dependent Endocytosis of Nanoparticles. *Adv Mater* **2009,** *21*, 419-424.
50. Nagai, Y.; Akashi, S.; Nagafuku, M.; Ogata, M.; Iwakura, Y.; Akira, S.; Kitamura, T.; Kosugi, A.; Kimoto, M.; Miyake, K., Essential role of MD-2 in LPS responsiveness and TLR4 distribution. *Nat Immunol* **2002,** *3* (7), 667-672.
51. de Belder, A. N.; Wik, K. O., Preparation and properties of fluorescein-labelled hyaluronate. *Carbohydr Res* **1975,** *44* (2), 251-257.
52. Alestrom, P.; D'Angelo, L.; Midtlyng, P. J.; Schorderet, D. F.; Schulte-Merker, S.; Sohm, F.; Warner, S., Zebrafish: Housing and husbandry recommendations. *Lab Anim* **2019**, 23677219869037.
53. Ellett, F.; Pase, L.; Hayman, J. W.; Andrianopoulos, A.; Lieschke, G. J., mpeg1 promoter transgenes direct macrophage-lineage expression in zebrafish. *Blood* **2011,** *117* (4), e49-56.
54. Bussmann, J.; Bos, F. L.; Urasaki, A.; Kawakami, K.; Duckers, H. J.; Schulte-Merker, S., Arteries provide essential guidance cues for lymphatic endothelial cells in the zebrafish trunk. *Development* **2010,** *137* (16), 2653-2657.
55. Hogan, B. M.; Herpers, R.; Witte, M.; Helotera, H.; Alitalo, K.; Duckers, H. J.; Schulte-Merker, S., Vegfc/Flt4 signalling is suppressed by Dll4 in developing zebrafish intersegmental arteries. *Development* **2009,** *136* (23), 4001-4009.
56. Varshney, G. K.; Pei, W.; LaFave, M. C.; Idol, J.; Xu, L.; Gallardo, V.; Carrington, B.; Bishop, K.; Jones, M.; Li, M.; Harper, U.; Huang, S. C.; Prakash, A.; Chen, W.; Sood, R.; Ledin, J.; Burgess, S. M., High-throughput gene targeting and phenotyping in zebrafish using CRISPR/Cas9. *Genome Res* **2015,** *25* (7), 1030-1042.
57. Carrington, B.; Varshney, G. K.; Burgess, S. M.; Sood, R., CRISPR-STAT: an easy and reliable PCR-based method to evaluate target-specific sgRNA activity. *Nucleic Acids Res* **2015,** *43* (22), e157.
58. Thisse, C.; Thisse, B., High-resolution in situ hybridization to whole-mount zebrafish embryos. *Nat Protoc* **2008,** *3* (1), 59-69.
59. Weinstein, B. M.; Stemple, D. L.; Driever, W.; Fishman, M. C., Gridlock, a localized heritable vascular patterning defect in the zebrafish. *Nat Med* **1995,** *1* (11), 1143-1147.
60. Schindelin, J.; Arganda-Carreras, I.; Frise, E.; Kaynig, V.; Longair, M.; Pietzsch, T.; Preibisch, S.; Rueden, C.; Saalfeld, S.; Schmid, B.; Tinevez, J. Y.; White, D. J.; Hartenstein, V.; Eliceiri, K.; Tomancak, P.; Cardona, A., Fiji: an open-source platform for biological-image analysis. *Nat Methods* **2012,** *9* (7), 676-682.
61. Schneider, C. A.; Rasband, W. S.; Eliceiri, K. W., NIH Image to ImageJ: 25 years of image analysis. *Nat Methods* **2012,** *9* (7), 671-675.

62. Askes, S. H. C.; Bossert, N.; Bussmann, J.; Talens, V. S.; Meijer, M. S.; Kieltyka, R. E.; Kros, A.; Bonnet, S.; Heinrich, D., Dynamics of dual-fluorescent polymersomes with durable integrity in living cancer cells and zebrafish embryos. *Biomaterials* **2018,** *168*, 54-63.